



Antibiofilm and antithrombotic hydrogel coating based on superhydrophilic zwitterionic carboxymethyl chitosan for blood-contacting devices

Dong Uk Lee^a, Mukhammad Kayumov^b, Junghun Park^a, Se Kye Park^a, Yeongkwon Kang^c, Yejin Ahn^d, Woojin Kim^a, Seung Hwa Yoo^e, Jun-Kyu Park^f, Bong-Gi Kim^d, Yong Suk Oh^g, In-Seok Jeong^{b,*,**}, Dong Yun Choi^{a,*}

^a Biomedical Manufacturing Technology Center, Korea Institute of Industrial Technology, Yeongcheon, 38822, Republic of Korea

^b Department of Thoracic and Cardiovascular Surgery, Chonnam National University Hospital and Medical School, Gwangju, 61469, Republic of Korea

^c Research Institute of Advanced Materials, Seoul National University, Seoul, 08826, Republic of Korea

^d Department of Organic and Nano System Engineering, Konkuk University, Seoul, 05029, Republic of Korea

^e Department of Quantum System Engineering, Jeonbuk National University, Jeonju-si, 54896, Republic of Korea

^f IMT Inc., Gwangju, 61086, Republic of Korea

^g Department of Mechanical Engineering, Changwon National University, Changwon, 51140, Republic of Korea

ARTICLE INFO

Keywords:

Zwitterionic
Hydrogel
Blood-clotting
Antimicrobial
Sepsis

ABSTRACT

Blood-contacting devices must be designed to minimize the risk of bloodstream-associated infections, thrombosis, and intimal lesions caused by surface friction. However, achieving effective prevention of both bloodstream-associated infections and thrombosis poses a challenge due to the conflicting nature of antibacterial and antithrombotic activities, specifically regarding electrostatic interactions. This study introduced a novel biocompatible hydrogel of sodium alginate and zwitterionic carboxymethyl chitosan (ZW@CMC) with antibacterial and antithrombotic activities for use in catheters. The ZW@CMC hydrogel demonstrates a superhydrophilic surface and good hygroscopic properties, which facilitate the formation of a stable hydration layer with low friction. The zwitterionic-functionalized CMC incorporates an additional negative sulfone group and increased negative charge density in the carboxyl group. This augmentation enhances electrostatic repulsion and facilitates the formation of hydration layer. This leads to exceptional prevention of blood clotting factor adhesion and inhibition of biofilm formation. Subsequently, the ZW@CMC hydrogel exhibited biocompatibility with tests of *in vitro* cytotoxicity, hemolysis, and catheter friction. Furthermore, *in vivo* tests of antithrombotic and systemic inflammation models with catheterization indicated that ZW@CMC has significant advantages for practical applications in cardiovascular-related and sepsis treatment. This study opens a new avenue for the development of chitosan-based multifunctional hydrogel for applications in blood-contacting devices.

1. Introduction

Cardiovascular diseases are a major cause of death worldwide, accounting for an estimated 17.9 million deaths attributed to them (representing 32% of global deaths; World Health Organization reports) [1]. The high prevalence of cardiovascular diseases has contributed to a significant increase in the widespread utilization of cardiac catheterization procedures in hospitalized patients. These procedures have

proven effective in reducing both mortality and morbidity rates [2,3]. Peripherally inserted central catheters (PICCs), one of the most commonly used blood-contacting cardiovascular devices, are used primarily in persons who require prolonged intravascular therapy, such as total parenteral nutrition, chemotherapy regimens, and antibiotic therapy [3]. PICCs can remain inserted into the basilic, brachial, or cephalic veins of the arm for an extended therapy period (days or weeks) [4]. The prolonged insertion increases the risk of acute infections and

Peer review under responsibility of KeAi Communications Co., Ltd.

* Corresponding author.

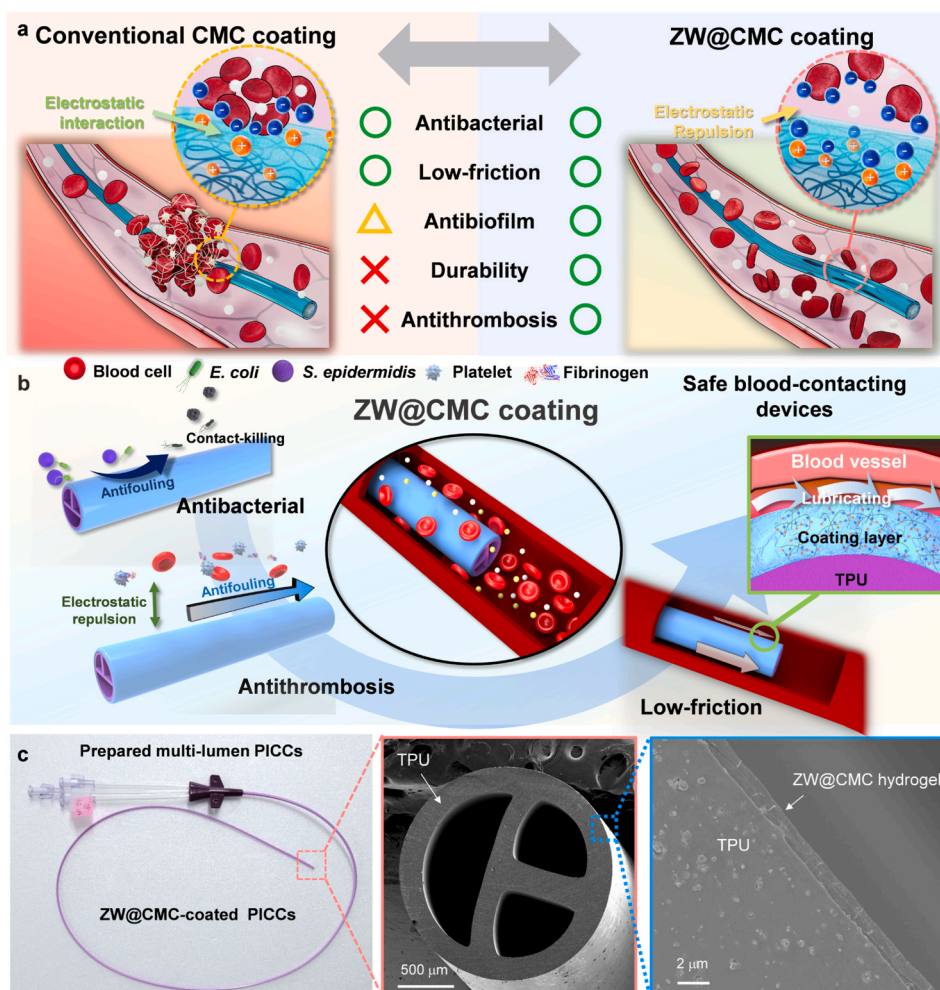
** Corresponding author.

E-mail addresses: isjeong1201@gmail.com (I.-S. Jeong), dychoi311@kitech.re.kr (D.Y. Choi).

<https://doi.org/10.1016/j.bioactmat.2023.12.009>

Received 30 July 2023; Received in revised form 11 December 2023; Accepted 11 December 2023

2452-199X/© 2023 The Authors. Publishing services by Elsevier B.V. on behalf of KeAi Communications Co. Ltd. This is an open access article under the CC BY-NC-ND license (<http://creativecommons.org/licenses/by-nc-nd/4.0/>).



Scheme 1. (a) Comparison of the novel multifunctional ZW@CMC coating with conventional CMC coating for blood-contacting devices (Green circles, yellow triangle and red ex marks represent good, moderate, and poor, respectively). (b) Schematic illustration of the multifunctional activities of the ZW@CMC layer. (c) Optical photograph of the prepared multi-lumen PICCs, and microscopic image of the ZW@CMC coating on PICCs.

thrombosis, rendering PICCs susceptible to catheter-associated bloodstream infections (CABSI) or thrombi with blood clotting [3,5]. Despite the implementation of sepsis treatment and anticoagulant administration to mitigate infection and thrombosis, PICC-related infections and thrombosis remain prevalent and pose significant risks to patients undergoing PICC therapy [6]. Furthermore, there is a need for reduced surface friction during tube insertion in PICC therapy to prevent blood vessel injury, as high surface friction between the tube and blood vessels causes unexpected movements during the cardiac catheterization process, leading to blood vessel injury, hemorrhage, and arterial spasms [7, 8]. To address these challenges, it is necessary to minimize the incidence of CABSI, thrombosis, and surface friction for the safe utilization of catheter devices.

Various strategies, such as the use of antimicrobial peptides, silver, and chitosan, have been suggested to control the microbial colonization of catheter surfaces and thereby prevent the occurrence of CABSI [9–11]. These materials exhibit potent antimicrobial activity attributed to their positively charged surfaces, which trigger bactericidal mechanisms involving the disruption of bacterial cell walls and interaction with intracellular components [12]. However, the utilization of positively charged surfaces in medical devices that come into contact with blood [13,14], as they could be susceptible to thrombus formation [15, 16] by means of electrostatic interactions with the dominant blood clotting factors (such as platelets, thrombin, and fibrinogen), which possess a net negative charge. Therefore, caution must be exercised in

employing positively charged surfaces in such applications [17–19]. Hence, the development of a biocompatible bifunctional material for highly efficient antimicrobial and antithrombotic coatings remains challenging.

O-Carboxymethyl chitosan (CMC), a chitosan derivative, is a promising coating material for blood-contacting catheter devices owing to its outstanding physicochemical properties, including non-toxicity, biodegradability, and biocompatibility [20]. The negatively charged carboxymethyl group of CMC exhibits antithrombotic properties similar to heparin by inducing electrostatic repulsion with negatively charged blood clotting components [21]. CMC possesses intrinsic antibacterial activity derived from the NH_3^+ groups of the chitosan structure, and exhibits better biocidal performance than chitosan owing to the abundance of cationic groups [22]. However, the presence of large cationic sites in CMC hinders its ability to exhibit antithrombotic performance owing to electrostatic interactions with blood clotting factors. This interaction has the potential to enhance blood clot formation, limiting the effectiveness of CMC as an antithrombotic coating material [23].

Zwitterionic polymers are known to have remarkable antithrombotic properties owing to the combined effects of electrostatic and steric repulsion of the hydration layer, resulting from the attraction of two ionic functional groups to water molecules [24,25]. Wu et al. demonstrated that the hydration characteristics of zwitterionic sulfobetaine result in ~8-fold stronger interactions with water molecules compared to polyethylene glycol. This enhanced interaction is attributed to the

presence of zwitterionic moieties (N^+ and SO_3^- groups) in sulfobetaine [26]. Furthermore, the anti-polyelectrolyte effect of the zwitterionic moieties introduces electrostatic repulsion against blood-clotting factors, resulting in good antifouling [27]. However, a zwitterionic polymer poses a practical risk of hydrophilic polymer embolism caused by polymer fragments from coating delamination [28].

In this study, we introduce a novel process for the synthesis of zwitterionic CMC (ZW@CMC) by utilizing biodegradable CMCs as antithrombotic and antibacterial hydrogel coatings, surpassing conventional CMC coatings (Scheme 1a). The ZW@CMC hydrogel serves as three primary functions: (i) prevention of bacterial infection, achieved through CMC-mediated bactericidal action and the formation of a hydration layer that inhibits fouling; (ii) thrombosis prevention, which can be attributed to the anti-adhesion of clotting factors via the hydration layer and electrostatic repulsion with the zwitterionic functional group; and (iii) vessel injury prevention, which can be attributed to the lubricating hydration layer (Scheme 1b) [29–31]. The inherent characteristics of ZW@CMC make it a highly promising biocompatible coating material with potential applications in various medical devices, including catheter tubes (Scheme 1c). The findings from this study contribute to the development of blood-contacting devices aimed at treating vascular diseases while minimizing the risks of infections, thrombosis, and friction-related vascular injuries.

2. Materials and methods

2.1. Preparation of TPU sheets and PICCs tubes

Thermoplastic polyurethane (TPU; TECHOTHANE™ TT-1095A, Lubrizol, USA) pellets were hot-pressed at 200 °C, 100 bar and then cooled to 25 °C to form 0.4 mm thick sheets using a gap gauge. Three-lumen PICC tubes were fabricated by extruding TPU pellets using a single-screw extruder (Davis-Standard, Pawcatuck, Connecticut, USA) for medical multi-lumen tubing. The extrusion process involved the following variables: screw speed of 16.5 rpm, die temperature of 195 °C, and barrel temperature of 205 °C (Fig. S1 and Table S1). The distal and proximal parts of the catheter tube had outer diameters of 5 Fr and 7 Fr, respectively. The surfaces of the as-prepared sheets and tubes were cleaned using 70% ethanol, following which the samples were thoroughly dried at 50 °C.

2.2. Preparation of zwitterionic CMC

One hundred microliter of CMC (10 cP viscosity, Bonding Chemical, Katy, Texas, USA) solution (2 wt%) was vigorously mixed with 1.3 g of 2-(diethylamino)ethyl chloride hydrochloride (DEAC; TCI, Chuo-ku, Tokyo, Japan) to prepare a completely dissolved solution. Sodium hydroxide (NaOH, 1 M; Duksan, Ansan, Republic of Korea) solution was added to the mixture to adjust the pH to 10, and then stirred at 300–400 rpm overnight. The mixture was purified with acetone three times via precipitation to obtain white precipitated DEAC@CMC particles. The precipitated DEAC@CMC particles were added to 100 mL of a hydrochloric acid (HCl; Duksan) solution (0.15 M) and completely dissolved at 40 °C. The DEAC@CMC solution was supplemented with excess amount of 1,3-propanesultone (0.85 g; TCI) and stirred at 300–400 rpm overnight at 40 °C to produce zwitterion-modified CMC (ZW@CMC, Fig. S2). The ZW@CMC solution was purified using benzoylated dialysis tubing (MWCO 2000, Sigma-Aldrich, St. Louis, Missouri, USA) for three days. Subsequently, the ZW@CMC solution was freeze-dried and stored at 5 °C for future use.

2.3. Preparation of the CMC and ZW@CMC coatings

The coating solution was prepared by mixing 2% sodium alginate (SA) and 2% CMC or ZW@CMC under vigorous stirring (3000 rpm) using an overhead mechanical stirrer. The TPU catheter tube was treated

with O_2 plasma for 10 min. The O_2 plasma-treated TPU catheter was then dipped into an acrylamide solution (1% w/v) for 1 h after being washed with distilled water. The washed TPU catheter was then dipped into the coating solution. Ultimately, the coated layer was crosslinked using a 1% w/v CaCl_2 solution for 1 min, followed by extensive rinsing with distilled water to eliminate any unreacted calcium ions from the coating. Subsequently, the coated material was thoroughly dried at 50 °C in a convection oven. Unless stated otherwise, the CMC and ZW@CMC hydrogel coatings contained SA.

2.4. Characterization

The structures of the prepared PICCs were confirmed using optical microscopy (AM7025X, Dunwell Tech. Inc., Torrance, California, USA) and a micro-CT scanner (Phoenix v|tome|x m; Waygate Technologies, Hürth, Germany). To analyze the surfaces of the coated specimens, attenuated total reflection Fourier transform infrared (FT-IR; Spectrum Two, PerkinElmer, Waltham, Massachusetts, USA) was conducted using a diamond crystal kit with a resolution of 4 cm^{-1} and 32 scans, generating spectra ranging from 650 to 4000 cm^{-1} . X-ray photoelectron spectroscopy (XPS) was carried out using an X-ray photoelectron spectrometer (Nexsa™, Thermo Fisher Scientific) with an Al K-alpha source (1486.6 eV) in the range of 0–1450 eV and at an angle of 90°. To characterize the morphology of the coated TPU films, scanning electron microscopy (SEM; SU8230, Hitachi Ltd., Hitachi, Ibaraki, Japan) was performed at an accelerating voltage of 5 kV. The surface roughness was measured using atomic force microscopy (AFM, xe-100, Suwon, Republic of Korea) in the non-contact mode. Kelvin probe force microscopy (KPFM) measurements were performed using a NanoScope V Multimode 8 atomic force microscope system and an SCM-PIT-V2 probe (Pt/Ir-coated probe; Bruker Corporation, Billerica, MA, USA) at the Korea Basic Science Institute (Jeonju Center, Republic of Korea).

The hydrophilicity of CMC and ZW@CMC hydrogels was assessed by static contact angle and captive bubble method using drop shape analyzer (DSA100, KRUSS GmbH, Germany). The swelling properties of the CMC and ZW@CMC hydrogels were investigated by immersion in deionized water. The swollen samples were retrieved at specified intervals, excess water on their surfaces was removed, and the final weight was measured. The water-absorption ratio was calculated using the following equation:

$$\text{Water absorption ratio (\%)} = \frac{M_f - M_o}{M_o} \times 100$$

where M_f and M_o are the weights before and after the CMC and ZW@CMC hydrogels, respectively.

2.5. In vitro antimicrobial test

Antibacterial characteristics were analyzed using the gram-negative bacterium *Escherichia coli* [*E. coli*; Catalog No. 11229; American Type Culture Collection (ATCC), Manassas, Virginia, USA] and the gram-positive bacterium *Staphylococcus epidermidis* (*S. epidermidis*; Catalog No. 12228; ATCC). *E. coli* was incubated in tryptic soy broth [containing 1.7% tryptone peptone and 0.3% phyton peptone (Thermo Fisher Scientific, Waltham, Massachusetts, USA) with 0.25% dextrose, 0.5% sodium chloride, and 0.25% dipotassium hydrogen phosphate (Sigma-Aldrich) at 37 °C in a shaking incubator. *S. epidermidis* was incubated in nutrient broth (Thermo Fisher Scientific) at 37 °C in a shaking incubator. Once the bacterial suspension reached an optical density of ~ 0.8 at a wavelength of 600 nm, the number of cells was determined using plate count agar. The TPU, CMC-, and ZW@CMC-coated films were cut into $30 \text{ mm} \times 30 \text{ mm}$ square shapes and cleaned with ethanol. The cell stock was diluted to a density of 1.0×10^6 [colony-forming units (CFU)] mL^{-1} and inoculated into washed films. The cells were covered with a cover glass ($22 \text{ mm} \times 22 \text{ mm}$) and incubated at 37 °C for 2 h. The inoculated

bacteria were collected in 5 mL of medium in a 50 mL conical tube. The collected cells were counted on plate count agar, and the antimicrobial efficiency was calculated using the following equation:

$$\text{Antimicrobial efficiency (\%)} = \left(\frac{N_{\text{control}} - N_{\text{sample}}}{N_{\text{control}}} \right) \times 100$$

where N_{control} is the number of cells in the control (untreated) and N_{sample} is the number of cells in the samples. The experiments were conducted in triplicate, and the data are reported as mean with standard deviation.

2.6. Biofilm inhibition test

To prepare the biofilm-inhibition testing stock, *E. coli*, *S. epidermidis*, methicillin-resistant *staphylococcus aureus* (MRSA; Catalog No. 43300; ATCC) and methicillin-susceptible *staphylococcus aureus* (MSSA; Catalog No. 6538; ATCC) were diluted to a density of 1.0×10^8 CFU mL⁻¹ in fresh media. Each specimen was placed in a 50 mL conical tube containing 20 mL of the bacteria-containing stock solution. The biofilms of *E. coli*, MRSA (and MSSA), *S. epidermidis* were grown in an incubator at 37 °C under static conditions for 48, 72 and 80 h, respectively. The biofilm-forming specimens were washed three times with phosphate-buffered saline (PBS) and stained with Acridine Orange solution for 30 min. Biofilm measurements were performed using a confocal microscope (LSM 700, Zeiss, Oberkochen, Baden-Württemberg, Germany) with a 20 × lens and 160 μm stack scan mode (scanned at a step size of 1.5 μm). A fluorescent image was obtained using a laser wavelength of 488 nm (illumination intensity of 10 mW) and a cutoff wavelength below 500 nm to remove the backlight.

2.7. In vitro antithrombosis analysis

Bovine serum albumin (BSA, fluorescein conjugate, Thermo Fisher Scientific) and fibrinogen (fibrinogen from human plasma, Alexa Fluor™ 488 conjugate, Thermo Fisher Scientific) were diluted in a PBS solution to a concentration of 0.1 mg mL⁻¹. The films (3 cm × 3 cm) were immersed in protein solutions at 37 °C for 24 h. The protein-attached films were washed twice with 10 mL of PBS to remove non-adhered proteins and then dried in air. Specimens were dried for 1 h. The adhesion of BSA and fibrinogen was confirmed using a fluorescence microscope with a 488 nm laser (illumination intensity of 10 mW). The 420–550 nm fluorescence was cut off to remove background light. The plasma adhesion test was conducted using human plasma (Catalog No. P9523, Sigma-Aldrich) with clotting factors of thrombin and fibrinogen in PBS (1 mg mL⁻¹). Note that this human plasma product is obtained from whole human blood, with platelets and blood cells removed. The specimens were then immersed in a plasma solution for 2 h at 37 °C. After washing with PBS, the specimens with foulants were fixed by treatment with a 2.5% glutaraldehyde solution for 2 h and then immersed in 50, 70, 80, 90, and 100% (v/v) ethanol solutions, in sequence, for dehydration. Finally, the treated substrates were dried in air, and the platelets that adhered to the film surface were observed using SEM.

The platelet and activated platelet adhesion tests were performed according to a previously reported study [32]. Briefly, platelet-rich plasma (PRP) was collected from citrated sheep whole blood via centrifugation. The blood reagents were purchased from Kisanbio (Seoul, Republic of Korea). This PRP was then diluted in a 1:4 ratio with a solution comprising 0.9% NaCl and 5 mmol L⁻¹ MgCl₂. To activate the platelets, adenosine 5'-diphosphate (10 μmol L⁻¹; Sigma-Aldrich, Catalog No. A2754) was introduced to the PRP at a 1:1 vol ratio. A 300 μL aliquot of the PRP solution was then applied to the TPU and hydrogel-coated specimens (2 cm × 2 cm) and incubated for 1 h. Unattached platelets were then rinsed three times with a 0.9% NaCl solution. Next, a buffer solution with a pH of 5.4 was prepared, consisting of sodium citrate (0.1 mol L⁻¹), citric acid (0.1 mol L⁻¹), and triton X-100

(0.1%). The *p*-nitrophenyl-phosphate was added to this buffer to reach a final concentration of 1 mg mL⁻¹. Subsequently, 840 μL of this buffer solution was then added into the sample with the adhered PRP and incubated for 40 min. After that, the incubation was terminated by adding 600 μL of a 2 mol L⁻¹ NaOH solution. The degree of PRP platelet adhesion rate to the surface was determined by measuring the absorbance at 405 nm using a UV-vis spectrophotometer (UV-2600i, Shimadzu, Japan).

Antithrombosis test was conducted using catheter specimens dipped in citrated sheep whole blood at 37 °C for 9 h. The procedures for washing and dehydrating were the same as those that were previously reported for the plasma adhesion test [33]. SEM was used to observe blood adhesion. The effects of the hydrogel coating on activated partial thromboplastin time (APTT) and prothrombin time (PT) were evaluated using a coagulometer (Thrombostat 1, Behnk Elektronik, Norderstedt, Germany), with APTT and PT testing reagents sourced from Fisher Diagnostics (Middletown, OH, USA). The plasma was obtained from the supernatant of citrated sheep whole blood, centrifuged at 2400 rpm for 10 min.

2.8. Computational details

The geometries of the molecules considered in this study were preliminarily optimized using the built-in Merck Molecular Force Field (MMFF94) and Avogadro software [34]. The molecular electrostatic potential (MEP) was calculated using the Gaussian 09 program and density functional theory. The MEP calculation used each monomer unit; the CMC was calculated using the B3LYP/6-31g (d) basis set [35], and ZW@CMC was calculated using the B3LYP/6-311g+ (d, p) basis set [36] with geometry optimization.

2.9. Cytotoxicity test

The *in vitro* cytotoxicity of the ZW@CMC-coated specimens was analyzed using C2C12 cells (Catalog No. CRL-1772; ATCC), which is a subclone of the mouse myoblast cell line (Fig. S3). The TPU, CMC-, and ZW@CMC hydrogel-coated films were cut into rectangular shapes with dimensions of 4 mm × 5 mm and cleaned with ethanol. NiSO₄ (99.99%, Sigma-Aldrich), prepared at a concentration of 10 mg mL⁻¹ in the culture medium, was used as the positive control. Dulbecco's modified Eagle medium (DMEM; Catalog No. SH30243, HyClone, Marlborough, Massachusetts, USA) supplemented with 10% fetal bovine serum (Catalog No. 30-2020, ATCC) and 1% penicillin/streptomycin (Catalog No. SV30010; HyClone) was used to culture cells. The C2C12 cells were seeded in 96-well cell culture plates (5.0 × 10³ cells per well) and cultured, at 37 °C for 24 h in an atmosphere containing 5% CO₂, to adhere to the well surface. After attachment, the cells were incubated with untreated (control), TPU, CMC-, or ZW@CMC hydrogel-coated films and a NiSO₄ solution for 24 h. At each time point, the films were removed, and the Cell Counting kit-8 (CCK-8, Dojindo Laboratories, Kumamoto, Japan) reagent was applied to the cells at a ratio of 1:5 (CCK-8 reagent: DMEM) and incubated for 4 h. The absorbance of the samples was measured at 450 nm using a microplate reader (Synergy H1; BioTek, Winooski, Vermont, USA). The cell viability was calculated as follows:

$$\text{Cell viability (\%)} = \frac{A_{\text{sample}} - A_{\text{blank}}}{A_{\text{control}} - A_{\text{blank}}} \times 100$$

where A_{sample} is the absorbance of the sample, A_{blank} is the absorbance of the blank (containing DMEM and CCK-8 solutions), and A_{control} is the absorbance of the untreated sample (without films). The experiments were conducted in triplicate, and the data are reported as mean values with standard deviation. LIVE/DEAD cell images were obtained by staining with Acridine Orange/Propidium Iodide (Logos Biosystems, Anyang, Republic of Korea) fluorescent dye. After cell culture with the

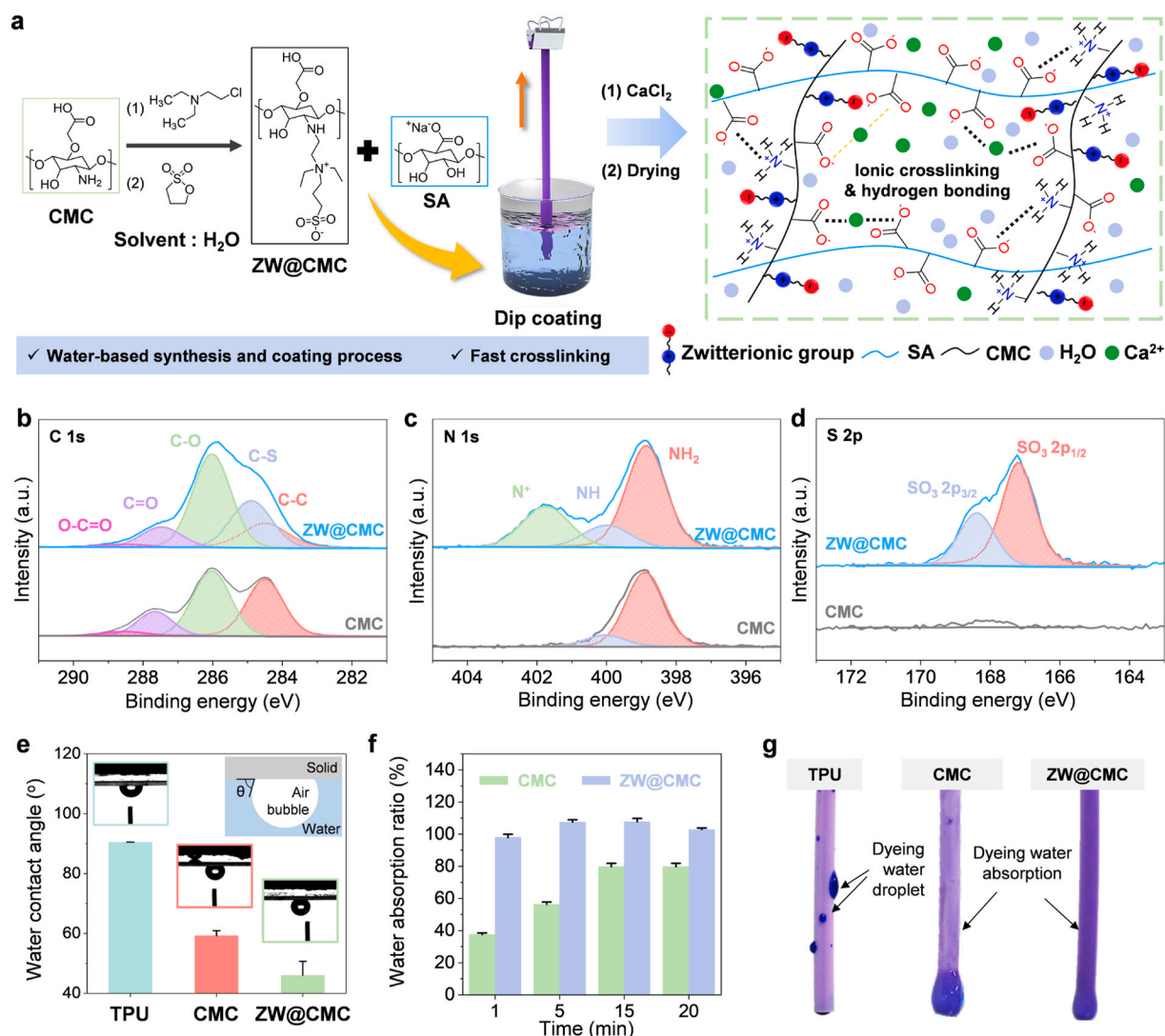


Fig. 1. (a) A schematic illustration of the synthesis procedure and hydrogel structure of ZW@CMC. (b–d) High-resolution XPS spectra of (b) C 1s, (c) N 1s, and (d) S 2p of CMC and ZW@CMC. (e) Contact angle measurement of hydrogel coatings using captive bubble method. (f) Time-dependent swelling ratio of the CMC and ZW@CMC coating. (g) Optical photograph of the water-absorption behaviors of the different catheter surfaces.

test films, the Acridine Orange/Propidium Iodide reagent was added to the media at a ratio of 1:50, and the cells were incubated at room temperature for 10 min. The intensity of the LIVE/DEAD cells was measured using an inverted fluorescence microscope (Eclipse Ti-u; Nikon, Tokyo, Japan).

2.10. Hemolysis test

The hemolytic activities of the materials were investigated referring to the ASTM F756 standard. Blood samples were freshly prepared and collected within 6 h. Each sample was added to the collected blood (diluted in PBS solution, 1:14 vol%) and incubated for 3 h at 37 °C. After incubation, the blood samples were transferred to microtubes and centrifuge 700 g for 15 min. Hemoglobin release was determined after centrifugation by photometric analysis of the supernatant at 540 nm using Drabkin's reagent (Sigma-Aldrich, mixed ratio 1:1 vol%).

2.11. In vivo antithrombosis test

Male Sprague-Dawley rats (11-week-old, 400–450 g, Samtako Bio Korea Co., Ltd., Osan City, Republic of Korea) were used in this study and received care in compliance with the Guide for the Care and Use of

Laboratory Animals. The rats were housed in temperature-controlled rooms with a 12 h light-dark cycle and standard food and water available. All surgical procedures were performed under sterile conditions. The animals were anesthetized with isoflurane (Hana Pharm Co., Ltd., Kyonggi-Do, Republic of Korea) and autobreathed during surgery. After the induction of anesthesia, a diagonal incision was made from the groin parallel to the inguinal ligament. The left femoral vein was isolated superior to the left epigastric vessels. The study catheter was carefully inserted through the femoral vein into the inferior vena cava at a length of 5 cm and fixed to the femoral vein using a 5-0 silk ligature. Two polypropylene sutures that were interrupted were used to seal the skin incision. After a week, the catheters were removed for additional examination.

2.12. In vivo antimicrobial test with bacteremia model

S. aureus was used to induce bacteremia in rats. Bacterial strains (MRSA; Catalog No. 43300; ATCC) were streaked onto blood agar plates and incubated for 16 h. Subsequently, a single colony was placed in Luria-Bertani broth and incubated. The cultured colonies were diluted and counted before injection. A total of 2.2×10^{10} bacterial strains were injected intravenously through the femoral vein before catheter

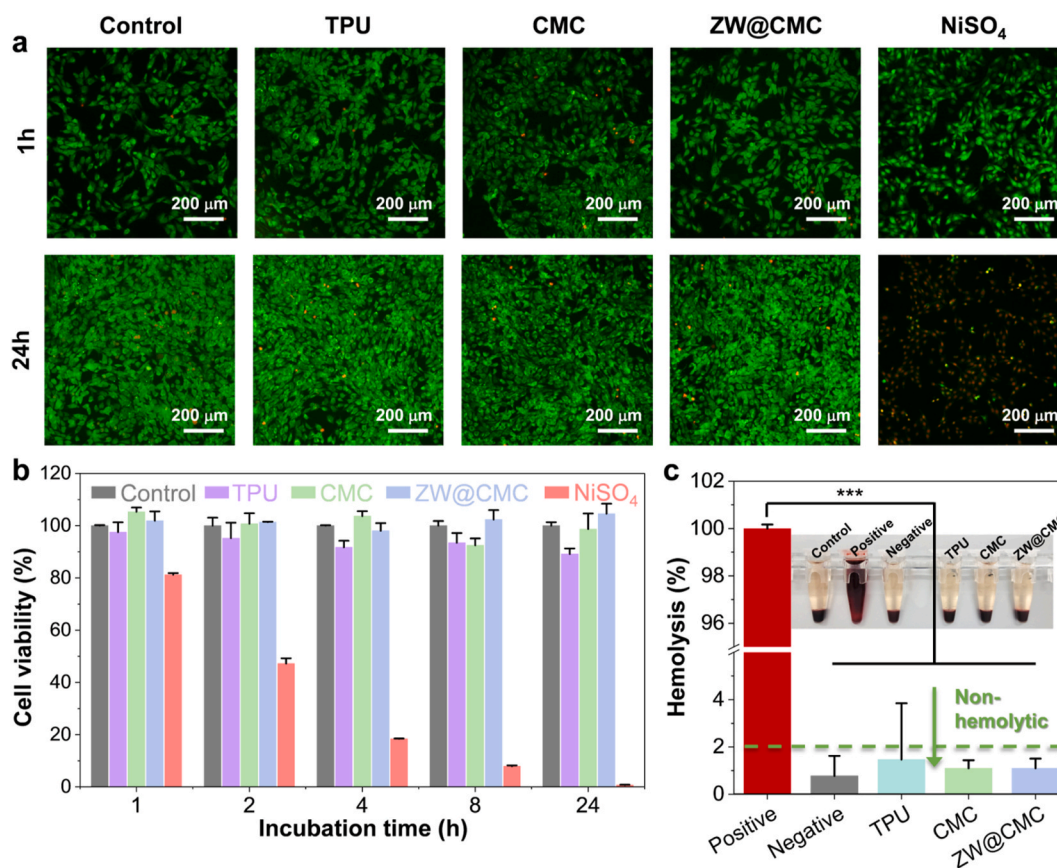


Fig. 2. (a) Microscopic fluorescence images of C2C12 myoblast cells after LIVE/DEAD cell staining. (b) Viability of C2C12 myoblast cells for different exposure times. (c) Hemolysis assay on erythrocytes with various materials ($n = 3$).

insertion. Complete Blood Count (CBC; Gem Premier 3000 with blood gas/electrolyte analyzer model 5700, Werfen Co., Barcelona, Spain), flow cytometry, and cell sorting (FACS; Beckman Coulter Inc., NAVIOS flow cytometer, California, USA) analyses were performed before and one day after the experiment to confirm the presence of bacteremia shock in the rats.

2.13. Catheter friction test

The catheter friction test was performed using an interventional device testing equipment (IDTE3000, Machine Solutions Inc., Flagstaff, Arizona, USA), which can measure the proximal and distal forces during the passage of a standard template according to the ASTM F2394-07 standard method (Fig. S4). The catheter friction test system equipped with the load cell (type 3482, Burster GmbH&Co. KG, Germany) was used to quantitatively determine the proximal push force required for trackability. Additionally, a catheter friction test was performed in a circulating PBS solution using an artificial cardiovascular system (Detachable Coronary Model, TrandoMed, Ningbo City, Zhejiang, China).

2.14. The durability test of the catheter coating layer

Hydrogel durability tests were performed using a force gauge (HF-1, Japan Instrumentation System Co., Ltd., Sakuraishi, Nara, Japan) equipped with a wet friction test system. The configuration of the wet friction test system is illustrated in Fig. S5. The TPU, CMC, and ZW@CMC hydrogel-coated catheters were fixed on a holder and rubbed onto flat pieces of PBS solution-drenched bovine aorta (obtained from a local butcher's shop) to simulate the blood vessel wall. All tests were conducted at a room temperature with a load of 0.3 N, velocity of 8 mm

s^{-1} , and stroke of 8 mm. To ensure the durability of the coating layer, each test was repeated a minimum of 1000 times.

2.15. Statistical analysis

All data were presented as mean \pm standard deviation unless otherwise specified. Statistical significance was evaluated using a two-tailed Student's *t*-test between different groups. The level of significance was labeled +, *, **, and ***, representing *p*-value <0.1 , <0.05 , <0.01 , and <0.001 , respectively.

3. Results and discussion

3.1. Design and characterization of zwitterionic CMC

The procedure for preparing the ZW@CMC hydrogel coating is summarized in Fig. 1a. The synthesized zwitterionic CMC polymer mixed with SA was rapidly coated on the surface with the ionic cross-linking of calcium chloride (Fig. S6) [37]. In particular, CMC or ZW@CMC are not stable under water and can dissolve easily because of its hydrophilicity. However, SA can crosslink with CMC or ZW@CMC through hydrogen and ionic bonds, resulting in a stable CMC or ZW@CMC hydrogel.

The zwitterionic CMC was synthesized via a water-based process using DEAC and 1,3-propanesultone (Fig. S2). The surface of the TPU needs pre-treatment before coating the ZW@CMC hydrogel (Fig. S7) due to the hydrophobic nature of the surface, which renders it unsuitable for coating with hydrophilic CMC or ZW@CMC. As chemical surface treatments may not be suitable for biomedical TPU materials due to their high chemical stability and biocompatibility, we conducted surface modification of TPU using O₂ plasma and subsequently treated it with an

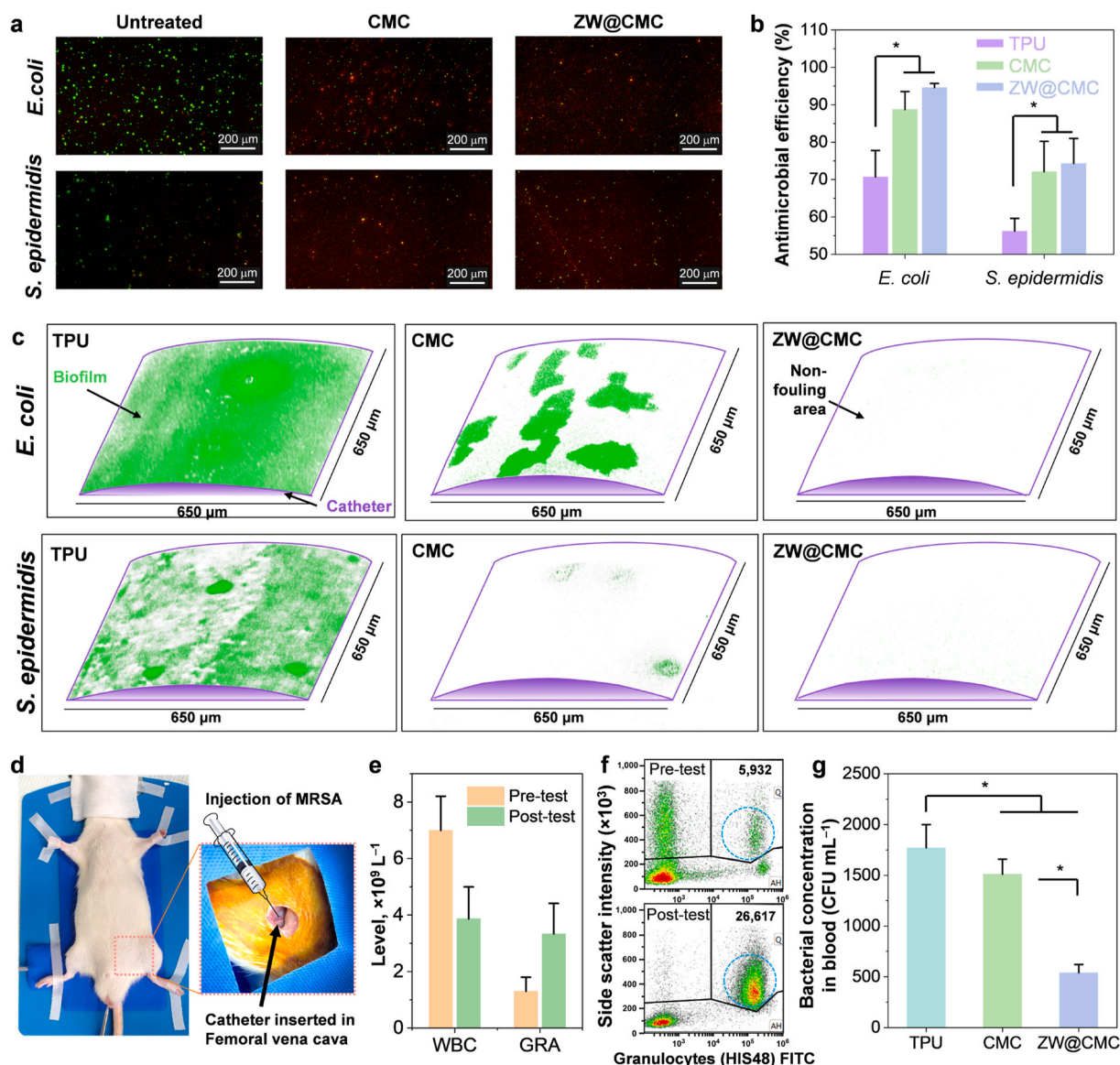


Fig. 3. (a) LIVE/DEAD bacterial staining assay comparing the efficiency of CMC and ZW@CMC solutions against *E. coli* and *S. epidermidis*. (b) Antimicrobial efficiencies of TPU, CMC, and ZW@CMC against *E. coli* and *S. epidermidis* ($n = 3$). (c) Antibiofilm activities of the TPU, CMC, and ZW@CMC coatings (green and white color represent biofilm- and non-fouling regions of the catheter surface, respectively). (d) Design of sepsis model test with systemic inflammation and antimicrobial catheter. (e) Complete blood count results and (f) flow cytometry and cell sorting results of the systemic inflammation model. (g) Bacterial counts of bacteremia blood after a day of sepsis model test ($n = 3$).

acrylamide solution (Fig. S8). Subsequently, a biocompatible coating solution of 2% SA and 2% ZW@CMC was coated onto the PICCs using the dip-coating method, followed by crosslinking with CaCl_2 . The carboxyl (COOH) functional group of SA facilitated the formation of a stable hydrogel layer by undergoing ionic bonding with the amine group of CMC and crosslinking with Ca^{2+} ions. The mechanical properties of the hydrogel layer are illustrated in Figs. S9–S12.

The synthesis of ZW@CMC hydrogel was confirmed via XPS measurements, as shown in Fig. 1b–d, S13a, and Table S2. The high-resolution C 1s spectra revealed that a C-S bond (284.9 eV) appeared in the synthesized ZW@CMC, which was not observed in CMC hydrogel (Fig. 1b) [38]. Furthermore, the high-resolution N 1s spectrum indicates an N^+ peak (401.75 eV) for sulfobetaine (Fig. 1c) [39]. The intensity of the C-OH/S-O bond in Fig. S13b was higher than that of CMC, indicating the presence of the sulfobetaine group of ZW@CMC [40,41]. The appearance of S 2p_{3/2} (168.4 eV) and S 2p_{1/2} (167.2 eV) peaks attributed to SO_3 demonstrated the synthesis of zwitterionic carboxymethyl chitosan (Fig. 1d) [39]. Additionally, the FT-IR spectra supported the

synthesis of ZW@CMC (Fig. S14). The successful synthesis of zwitterionic CMC using a water-based process with 1,3-propanesultone is demonstrated in this study.

To evaluate the antifouling performance of the hydrogel, it was important to investigate its hydrophilic properties. A fully wettable surface enables steric repulsion between the hydration layer containing sulfobetaine functional groups and foulants. As depicted in Fig. 1e, the water contact angle (WCA) was assessed using the captive bubble method to determine the surface wettability under wet conditions. The WCA values were approximately 90.45° for TPU, 59.23° for CMC and 46.0° for ZW@CMC. These WCAs of CMC and ZW@CMC hydrogels were relatively lower than those of TPU, demonstrating aerophobic surfaces due to their hydrophilic and hygroscopic characteristics (Fig. S15). The time-dependent water absorption ratio demonstrated the superior hygroscopic properties of the ZW@CMC hydrogel layer. The CMC hydrogel coating fully absorbed water within 15 min, whereas the ZW@CMC hydrogel was completely swollen within 1 min, indicating its superior water-absorption ability (Fig. 1f). The ZW@CMC hydrogel exhibited

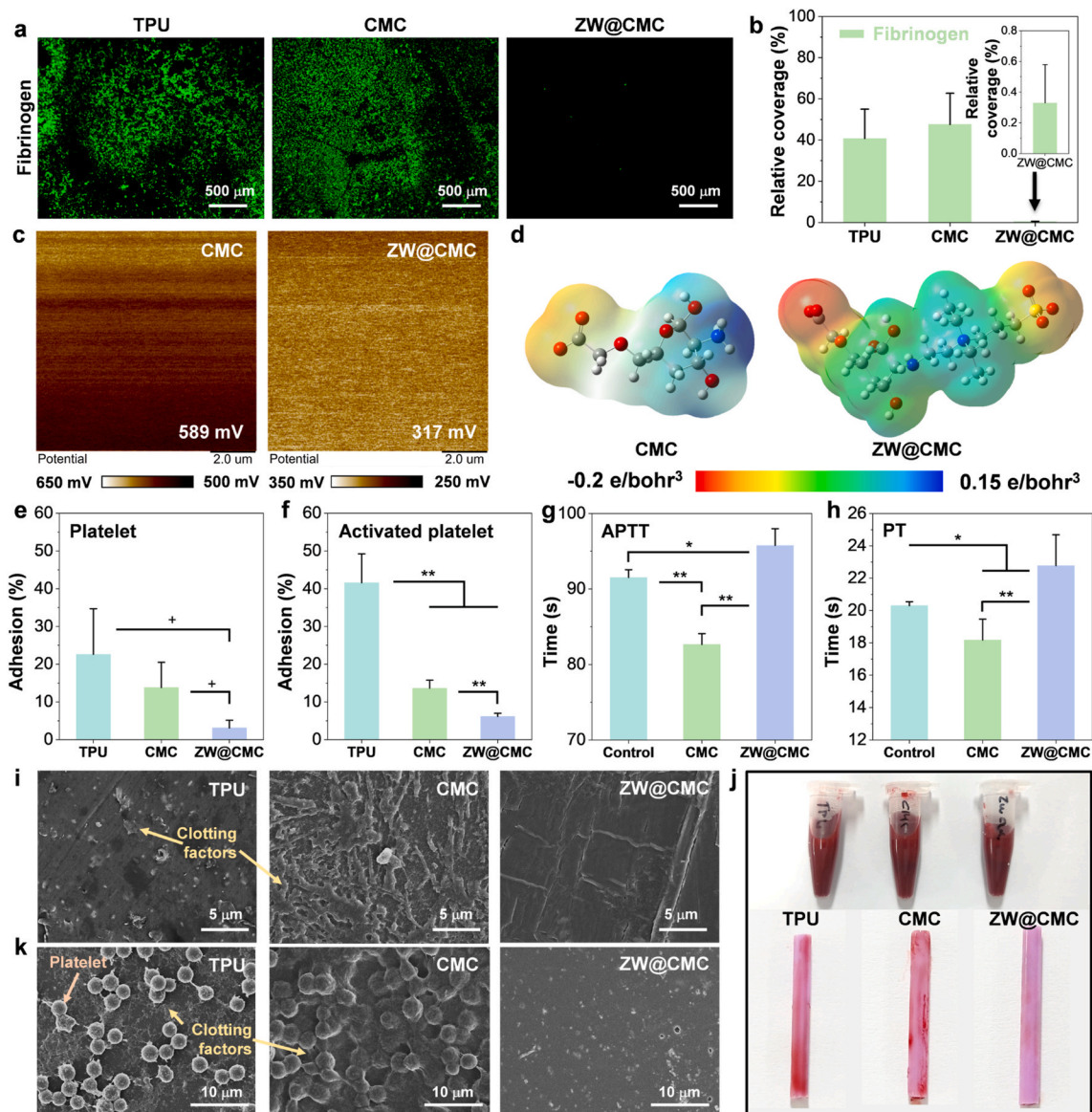


Fig. 4. (a) Fibrinogen adhesion on TPU, CMC-, and ZW@CMC-coated surfaces. (b) Relative extent of fibrinogen adhesion on different surfaces. (c) Surface potential measurement of the different surfaces using a Kelvin probe force microscope. (d) The molecular electrostatic potential map of CMC and ZW@CMC calculated using Gaussian 09 quantum mechanical calculation. Platelet adhesion test of (e) platelet and (f) activated platelet on the different surfaces ($n = 3$). Comparison of (g) activated partial prothrombin time (APTT) and (h) prothrombin time (PT) of plasma (control), CMC- and ZW@CMC-coated surfaces ($n = 4$). (i) Adhesion of clotting factor-active human plasma on different surfaces. (j) Optical images of blood adhesion on the different surfaces of PICCs. (k) SEM images of the *in vitro* antithrombosis test of citrated sheep whole blood against different surfaces.

enhanced hydrophilic and hygroscopic properties due to the efficient hydration facilitated by the ionic solvation of the zwitterionic sulfobetaine groups. To further demonstrate the outstanding wetting and hygroscopic properties of the hydrogel, we performed a dipping test in blue-dyed water for 5 s. As shown in Fig. 1g, the ZW@CMC-coated PICC tube exhibited a darker purple color because of the adsorbed dye water and the absence of dewetted water droplets. This clearly demonstrates the better hydration ability of ZW@CMC than those of pristine TPU and CMC.

3. 2. *In vitro* cytotoxicity test

Materials used in implantable blood-contacting medical devices must be toxicologically evaluated to ensure patient safety. Due to the high trade-off between antibacterial efficacy and toxicity in the human body associated with these devices, it is crucial to conduct thorough

investigations in this regard. Therefore, *in vitro* cytotoxicity assay was conducted to evaluate the biosafety of ZW@CMC. The ZW@CMC-coated films were immersed in cultured C2C12 myoblasts for up to 24 h. To minimize physical damage to the cells during culture, the films were immersed obliquely in the culture medium in a well-plate. To confirm the reliability of the assay, a blank condition was employed as an assay control, and the TPU film and nickel sulfate (NiSO_4) were used as the negative and positive controls, respectively [42]. Cell images obtained after live/dead staining are shown in Fig. 2a. Live cells were stained green, while dead cells were stained red with Propidium Iodide. The positive control (NiSO_4) demonstrated intrinsic cytotoxicity, leading to cell death in the majority of cells. However, the other samples, including ZW@CMC, exhibited a notable increase in cell count. Fig. 2b illustrates the results of the cell viability tests. The ZW@CMC group showed high cell viability (104.6%), similar to that of the control, TPU, and CMC groups, upon incubation for 24 h. In contrast, extremely low cell

viability was observed in the positive control (0.7%).

Blood compatibility is a crucial consideration for the development of materials for blood-contacting devices. To assess the hemolytic potency of the ZW@CMC hydrogel on erythrocytes, a hemolysis test was conducted according to the ASTM F756 standard procedure. According to the ASTM F756 standard, a hemolysis index of less than 2% indicates non-hemolytic activity. As shown in Fig. 2c, ZW@CMC showed excellent hemocompatibility with a hemolytic activity of ~1.10%, similar to that of the negative control (polyethylene film, 0.78%), TPU (1.47%), and CMC (1.10%), whereas the positive control (Triton X-100) resulted in nearly 100% hemolysis. These results indicate the biocompatibility of ZW@CMC, as it does not exhibit any adverse effects on cells or erythrocytes. This makes it a promising material for potential applications in medical devices.

3.3. *In vitro* and *in vivo* tests of antimicrobial activities

The antimicrobial activities of CMC and synthesized ZW@CMC were investigated using a LIVE/DEAD bacterial assay (Fig. 3a). Live cells were stained green, whereas dead cells were stained red in the LIVE/DEAD bacterial assay. The CMC and ZW@CMC materials effectively killed most of the *E. coli* and *S. epidermidis* cells. Furthermore, they exhibited zones of inhibition against MRSA and MSSA (Figs. S16a and b). These results demonstrate their bactericidal properties and highlight their potential to mitigate bacterial infection risks associated with medical devices. Fig. 3b and S16c show the antimicrobial activities of TPU, CMC-, and ZW@CMC-coated films. For *E. coli*, the CMC- and ZW@CMC-coated films exhibited higher antimicrobial efficiencies of 88.7% and 94.6%, respectively, compared to the TPU film (~70%). For *S. epidermidis*, the CMC- and ZW@CMC-coated films displayed an antimicrobial efficiency of >70%, which was better than that of the TPU film (~56.2%). The antibacterial activity of TPU was significantly enhanced when coated with CMC and ZW@CMC hydrogels (p -value < 0.05), and these results were comparable to those of a previously reported study [43]. The CMC- and ZW@CMC-coated films demonstrated antimicrobial efficiencies of ~72.8% and ~71.5% against MSSA, and ~80.5% and ~79.8% against MRSA, respectively (Fig. S16c). Note that the results of antibacterial efficiency were obtained after a short incubation period of just 2 h on the film surface. Consequently, the antimicrobial activity of ZW@CMC-coated films remained consistent following the zwitterionic modification of CMC compared to CMC-coated films.

Fig. 3c and S17 show the results of biofilm tests conducted to determine the antibiofilm effectiveness of ZW@CMC in preventing CABSIs. Biofilms of *E. coli* and *S. epidermidis* were abundantly formed on the surfaces of the non-coated TPU tubes, whereas the CMC- and ZW@CMC-coated specimens exhibited biofilm inhibition. In contrast to the CMC-coated specimens, the ZW@CMC-coated specimens demonstrated remarkable biofilm inhibition activities against both *E. coli* and *S. epidermidis*. This antibiofilm effect of ZW@CMC hydrogel coating was also evident against MSSA and MRSA, as shown in Fig. S16d. Its superior hydration capability and bactericidal activity resulted in a greater inhibition of biofilm formation compared to the CMC hydrogel.

During medical procedures, catheters are susceptible to infection and serve as a source of bacterial contamination. Moreover, bacteria can grow and adhere to the catheter surface during bacteremia, potentially aggravating sepsis. Therefore, the *in vivo* antimicrobial activities of CMC and ZW@CMC were evaluated using a developed sepsis model with the insertion of coated catheters. As depicted in Fig. 3d, an MRSA suspension was injected into the femoral vein after catheter insertion. The developed bacteria-induced systemic inflammation confirmed that the rats exhibited sepsis, as indicated by an increase in the level of granulocytes (GRA) occurrence with a decrease in the white blood cell (WBC) count, as determined via a CBC test (Fig. 3e). Furthermore, an increase in the number of granulocytes (Fig. 3f) and total immune cells (Fig. S18) was measured using FACS, indicating the occurrence of bacteremia. Fig. 3g demonstrates the antimicrobial efficacy of the coated catheters

for sepsis treatment, based on a model of catheter insertion during bacteria-induced systemic inflammation. After 24 h of the systemic inflammation model with catheterization, ZW@CMC showed a relatively decreased bacterial concentration in the bacteremia compared to the CMC- (reduction of 64.24%) and TPU-contacted blood (reduction of 69.49%). Overall, these results suggest that the ZW@CMC coatings with good antimicrobial properties can inhibit bacterial infection and support sepsis treatment, leading to their application in blood-contacting devices.

3.4. *In vitro* antithrombotic activities

Proteins, such as fibrinogen, contribute to procoagulant activity, promoting platelet adhesion and increasing the risk of thrombosis. Thrombin and activated platelets convert fibrinogen into fibrin, initiating blood clot formation. Consequently, the use of an antithrombotic coating is essential to prevent the accumulation of fibrinogen and other blood clotting factors, which represent the initial stages of thrombosis development. Fig. 4a shows the fluorescence microscopy images of fibrinogen adhered to each film surface after exposure for 24 h. Remarkably, the superhydrophilic ZW@CMC hydrogel exhibited impressive antifouling properties against fibrinogen, contrasting with the TPU and CMC hydrogels (Fig. S19). One of reasons is that superhydrophilic hydrogels, capable of forming a hydration layer, possess steric repulsion forces impeding the adhesion of foulants, including substances responsible for blood clotting [44]. This is further supported by Fig. 4b, which illustrates the relative adhesion area extracted from the microscopic fluorescence images, thereby reinforcing these findings. The ZW@CMC hydrogel exhibited negligible area coverage of fibrinogen (0.33%), whereas the TPU (40.75%) and CMC (47.58%) hydrogels showed significantly higher adhesion areas.

Note that, despite the hydrophilic nature of the CMC hydrogel, it exhibited higher fibrinogen adhesion than what was observed with TPU [45]. This can be attributed to the interaction of the positively charged CMC surface with the net negatively charged fibrinogen (Fig. 4c and S20). The CMC hydrogel has a positive potential of 589 mV, whereas the TPU surface is negatively charged surface (−311.05 mV). The ZW@CMC hydrogel had a relatively low positive potential of 317 mV compared to that of the CMC, chitosan, and hyaluronic acid coatings. These surface potential results can be explained by the MEP map obtained by quantum mechanics calculations using Gaussian 09 (Fig. 4d). The MEP calculation was carried out only CMC and ZW@CMC without SA. In CMC, the COOH functional group had a charge density of $-0.15 e \text{ Bohr}^{-3}$, whereas N atom had that of $+0.15 e \text{ Bohr}^{-3}$. However, in ZW@CMC, the charge densities of the COOH functional groups, SO_3^- , and N atoms were -0.2 , -0.16 , and $+0.08 e \text{ Bohr}^{-3}$, respectively, indicating a relatively low positive charge [46]. In conclusion, the introduction of the negatively charged SO_3^- group in ZW@CMC resulted in a lower positive potential of the N atoms but an increased negative potential of COOH compared to CMC. These findings, combined with previous protein adhesion tests, provide stronger evidence supporting the excellent antithrombotic performance of ZW@CMC.

Platelets are conventionally defined as playing a vital role in hemostasis and thrombosis. Once a platelet adhered and activated, platelets secrete various clotting factors, resulting in occlusive thrombus formation, myocardial infarction, and stroke [47,48]. Hence, it is imperative for blood-contacting devices to prevent platelet and activated platelet adhesion. Fig. 4e and f depict the results of the adhesion test for platelets and activated platelets, respectively, demonstrating the antifouling performance of CMC and ZW@CMC hydrogel coatings. The ZW@CMC-coated surface exhibited the lowest percentage of adhered platelets at 3.10%, while the CMC-coated and TPU surfaces had larger percentages of 13.80% and 22.62%, respectively. For activated platelets, the anti-adhesion property of the ZW@CMC-coated surface (6.13%) outperformed that of the CMC-coated surface (13.64%), as expected. But, both the CMC-coated and ZW@CMC-coated surfaces exhibited

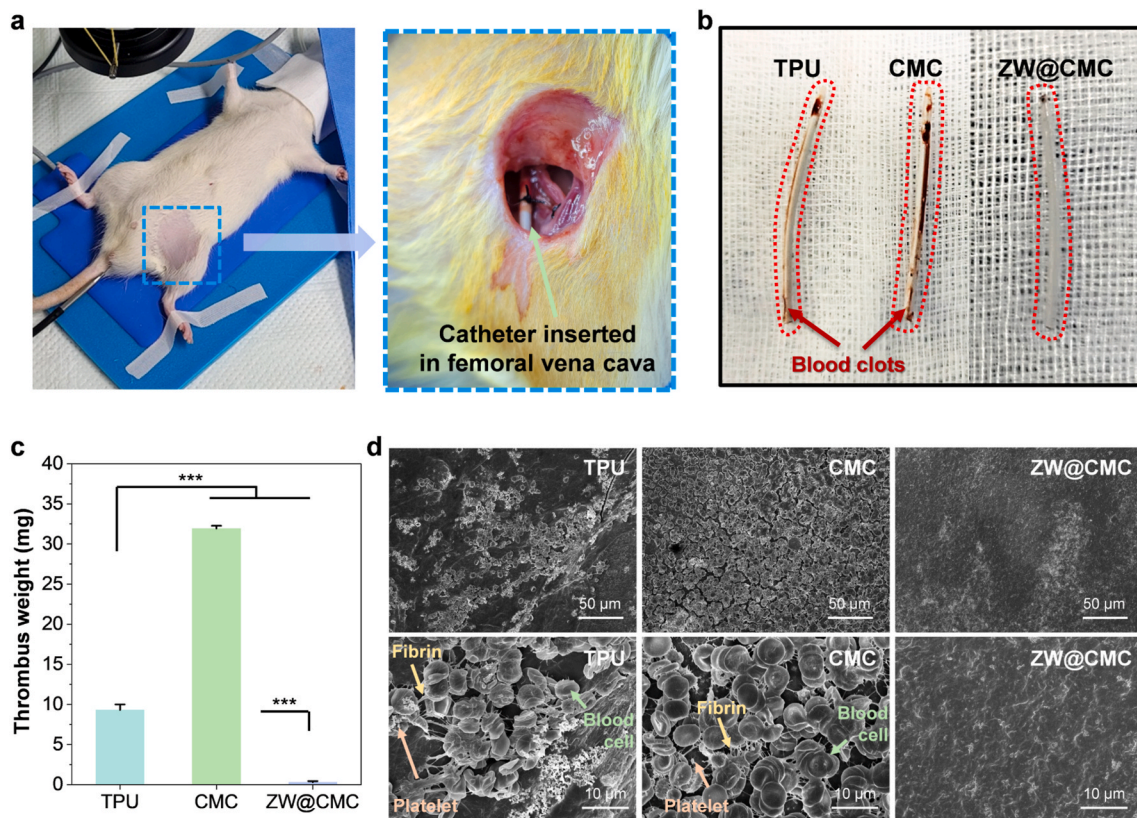


Fig. 5. *In vivo* assessment of the catheter antithrombotic performance. (a) Photographic image of the catheterization in femoral vena cava implantation model of rat. (b) Photographic images of the extracted catheters after 1 week of catheterization. (c) Weight of blood clots on the catheter surfaces in femoral vena cava implantation model after 1 week ($n = 3$). (d) SEM images of blood clots on the surfaces of the catheters.

significantly lower adhesion rates compared to the TPU surface (41.59%).

Platelets and artificial surfaces can support the initiation phase of coagulation by providing binding sites for prothrombin and factor XI, triggering the intrinsic pathway of thrombosis (Fig. S21) [49,50]. Therefore, the APTT tests were performed to quantitatively evaluate the antithrombotic performances of hydrogel-coated surfaces (Fig. 4g). The ZW@CMC-coated surface showed suppressed coagulation of the intrinsic pathway (95.77 s), in contrast to the control (91.53 s; plasma without coating) and the CMC-coated surface (82.65 s). Additionally, we conducted the PT tests to assess the extrinsic pathway of thrombosis (Fig. 4h). Tissue factor (TF) is recognized as the primary cellular initiator of blood coagulation (Fig. S21). Following vessel injury, the TF:FVIIa complex activates the coagulation protease cascade, leading to fibrin deposition and platelet activation [51]. This activated plasma then triggers factor X activation, leading to the extrinsic pathway of thrombosis [52]. The PT test results showed that the ZW@CMC-coated surface (22.78 s) prolonged the PT compared to the control (20.3 s) and the CMC-coated surface (18.18 s). The findings from the APTT and PT tests highlight a distinct contrast in the antithrombotic activities of CMC and ZW@CMC hydrogels. The extended clotting times observed in both APTT and PT tests for ZW@CMC can be attributed to its ability to suppress the adhesion of platelets and activated platelets. In contrast, the tendency of CMC to promote platelet adhesion resulted in shortened clotting times, as demonstrated by the APTT and PT results.

To further investigate the antithrombotic effect, an adhesion test was performed using platelet-free human plasma containing clotting factors (Fig. 4i and S22). Although the TPU surface has a negative charge, it promotes the adhesion of clotting factors because of hydrophobic interactions, which are important for inducing high protein-surface affinity [53]. Proteins tend to adhere more strongly to hydrophobic

surfaces than hydrophilic surfaces due to the hydrophobic interaction effect. Consistent with the results of the fibrinogen adhesion test and KPFM measurements, the CMC surface revealed many adhered clotting factors owing to its highly positive charge, whereas the ZW@CMC hydrogel showed no clotting factor adhesion.

Next, we performed an *in vitro* blood clotting test with citrated sheep whole blood to examine the antithrombotic performance under blood-contacting conditions. After 9 h of blood contact, the ZW@CMC-coated catheter surface showed nearly no adhesion of blood clots, whereas the surfaces of the TPU and CMC-coated catheters were covered with blood clots (Fig. 4j). SEM images show that blood clots with platelets and blood clotting factors adhered to the TPU, CMC, and ZW@CMC hydrogel surfaces (Fig. 4k and S23). Significant deposits of platelets and blood-clotting factors were observed on the surfaces of both the TPU and CMC-coated tubes. However, for the ZW@CMC hydrogel surface, a remarkable reduction in the adhesion of platelets and blood-clotting factors was observed. These results suggest the applicability of the ZW@CMC hydrogel coating to effectively inhibit thrombosis *in vivo*.

3.5. *In vivo* antithrombotic activities

A PICC is a medical device inserted into a vein or artery to provide access to medical treatments such as fluid administration, blood transfusions, or medication delivery. However, artificial polymeric substances in catheters pose a risk of thrombosis by promoting blood coagulation via intrinsic pathways when inserted into blood vessels, which can lead to complications, such as occlusion, pulmonary embolism, or swelling in the legs. The standard medical procedure to prevent blood clotting during the insertion of medical devices involves the use of anticoagulants, such as heparin. However, some patients may

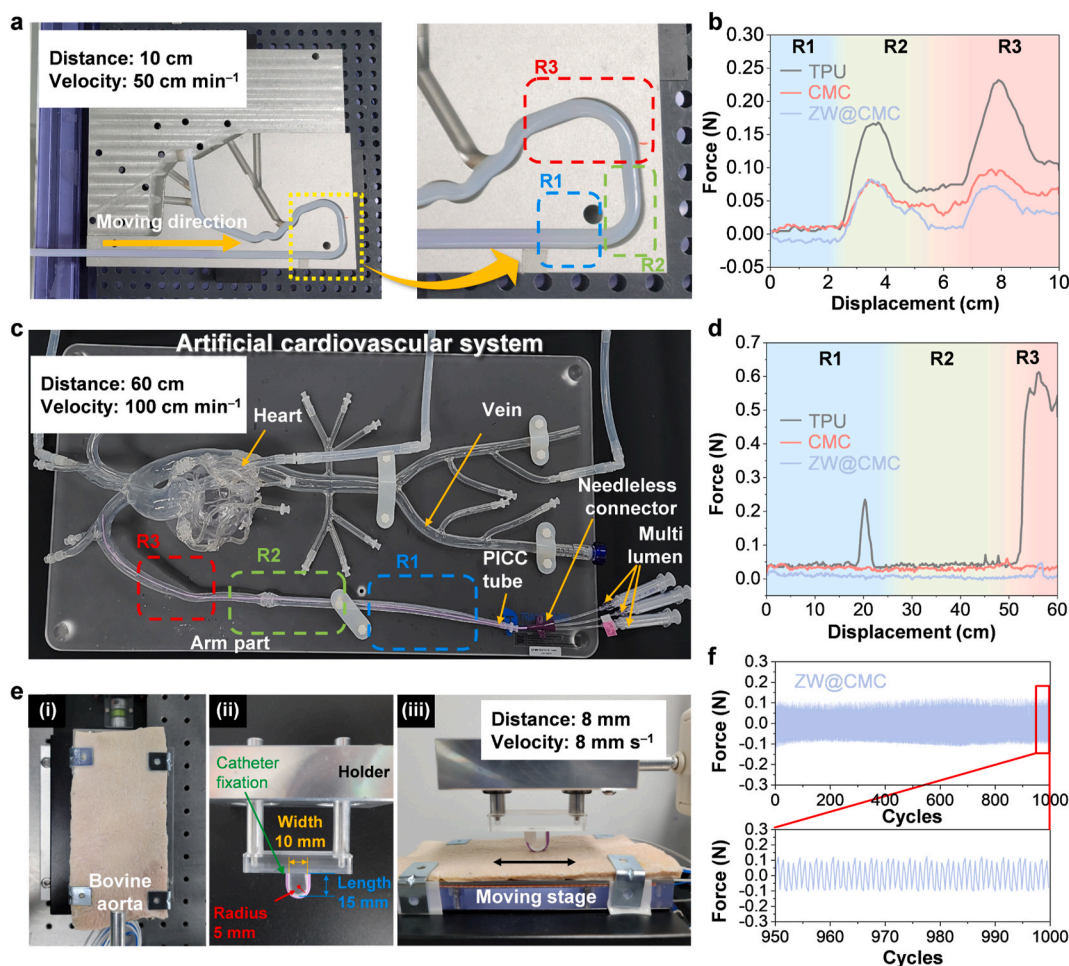


Fig. 6. (a) Photograph of the interventional devices testing equipment (IDTE) used to carry out the catheter friction test, with the passage of a standard template (ASTM F2394-07). (b) Results of the catheter friction test conducted with the IDTE. (c) Photograph of the artificial cardiovascular system model employed for simulating peripherally inserted central catheterization, during the catheter friction test. (d) Results of the peripherally inserted central catheterization simulation test. (e) Photograph of the wet friction test system. (f) Results of the cyclic wet friction test.

experience side effects such as bleeding, pain, and difficulty in breathing due to the use of anticoagulants. In such cases, antithrombotic coatings may be an important alternative for patients experiencing adverse effects.

To assess the antithrombotic performance of the ZW@CMC hydrogel, a catheter insertion experiment was conducted in the femoral vein of rats over a one-week period (Fig. 5a). As evidenced by the previous *in vitro* biocompatibility results (Fig. 3), the biocompatibility is further confirmed as the rats with femoral vein catheterization survived for a week after the procedure. Fig. 5b shows the extracted catheter after insertion into the femoral vein of the rats to confirm thrombus formation on the surface. Notably, the surface of ZW@CMC was quite clean compared to those of TPU and CMC. The results of the thrombus weight measurement in Fig. 5c distinctly show the superior antithrombotic ability of ZW@CMC compared with those of TPU (~96.77% reduction) and CMC (~99.06% reduction). As shown in Fig. 5d, the SEM images of blood clots on the surfaces clearly demonstrate antithrombosis of the coating layers via *in vivo* test, similar to the previously shown *in vitro* antithrombotic activities. The CMC-coated specimen showed numerous blood clots with platelets, blood cells, and fibrin formation owing to its intimacy with blood-clotting factors by electrostatic interactions compared to the control specimen. Moreover, the SEM image in Fig. S24 revealed the presence of multiple activated platelets adhering to the CMC surface, indicating its unsuitability as a coating material for blood-contacting devices. In contrast, ZW@CMC exhibited superior

performance. These findings underscore the effectiveness of ZW@CMC hydrogel in antithrombotic applications, potentially making it a more suitable choice for use in blood-contacting medical devices.

3.6. Catheter friction test

High vascular wall shear stress during catheterization can cause discomfort and tissue injury. Particularly during cardiac catheterization, damage to blood vessels near the heart can be life-threatening and may cause end-organ ischemia and hemorrhage [7,8,54]. Therefore, it is necessary to ensure the surface friction performance of catheter devices for safe vascular treatment.

A catheter trackability test was performed to measure the load of the catheter insertion, which reflected the surface friction properties, as shown in Fig. 6a. The proximal force was continuously measured when the catheter tube was inserted at a constant speed of 50 cm min^{-1} through the artificial vascular path of the Teflon tube. The three regions, R1, R2, and R3, represent the linear, curved, and rapidly curved paths, respectively (Fig. S25). Fig. 6b shows the insertion load versus displacement curves of the TPU, CMC-, and ZW@CMC-coated tubes. The maximum loads for the CMC- and ZW@CMC-coated tubes were significantly reduced to ~35.5% and 42.0%, respectively, compared to that of the non-coated TPU tube. The insignificant variation in the bending strength (Fig. S10b) implied that the load reduction was predominantly attributed to the low friction properties of the CMC or ZW@CMC

hydrogel.

The superior low-friction properties of the ZW@CMC hydrogel were further demonstrated through a more practical method using an artificial cardiovascular system model comprising of a silicon tube (Fig. 6c). The test sections in the arm vein of the cardiovascular model were divided into R1, R2, and R3 for slight, linear, and rapid curves, respectively. The non-coated TPU exhibited an undesirable shudder when inserted into the artificial cardiovascular model (Movie S1) because of its high surface friction. However, the ZW@CMC tube was smoothly inserted into the vein without any unsuitable perturbations (Movie S2). This effect was attributed to the ability of the ZW@CMC hydrogel to remarkably reduce the surface friction; the maximum loads for the CMC- and ZW@CMC-coated tubes were diminished by 90.19% and 92.28%, respectively, compared to the load of the TPU tube (Fig. 6d). These results highlight the outstanding potential of the ZW@CMC hydrogel coatings for PICC applications.

Supplementary video related to this article can be found at <https://doi.org/10.1016/j.bioactmat.2023.12.009>

The durability of the coatings was examined using cyclic wet friction tests (Fig. 6e). The bovine aorta, which was used as a vascular graft because of its biocompatibility with human blood vessels, was selected as the counter-friction material for the test (Fig. 6e i) [55]. The catheter tube holder for testing was prepared as shown in Fig. 6e ii. The catheter tube equipment had a length of 15 mm, a width of 10 mm, and a radius of 5 mm. The cyclic wet friction test was performed by applying a force of 0.3 N to the catheter tube, with the bovine aorta placed on a motorized stage moving a distance of 8 mm at a velocity of 8 mm s⁻¹ (Fig. 6e iii). The friction properties of the ZW@CMC hydrogel did not deteriorate during 1000 wet friction cycles (Fig. 6f). The durability of the ZW@CMC hydrogel coating was evident as it exhibited no observable damage, such as delamination or cracks, unlike the CMC hydrogel coating (Fig. S26).

4. Conclusion

In summary, in the present study, we successfully developed a biocompatible hydrogel coating, for blood-contacting medical devices, using ZW@CMC, a natural polysaccharide-derived material. The ZW@CMC hydrogel was fabricated using a water-based green process and exhibited excellent antimicrobial, antibiofilm, antithrombotic, and lubricating properties. We demonstrated that the ZW@CMC hydrogel could be rapidly ionically crosslinked and uniformly coated on PICCs made of medical-grade TPU. The mechanism underlying the antimicrobial and antithrombotic effects of ZW@CMC hydrogel can be described as follows: (1) the superhydrophilic and hygroscopic characteristics of the hydrogel allow for an increase in hydration formation; (2) the intrinsic antimicrobial properties of ZW@CMC allow for the inhibition of biofilm formation and an increase in antimicrobial performance; and (3) its high hygroscopic properties and negative electrostatic repulsion potential allow for the suppression of blood clotting. Furthermore, the hygroscopic properties of the developed hydrogel promote the formation of a hydration layer, leading to significantly reduced friction, as measured via catheterization simulations using an artificial cardiovascular system model. The novel ZW@CMC hydrogel coating developed in this study holds great promise for the development of multifunctional blood-contacting medical devices, including vascular catheters.

Data availability statement

The data that support the findings of this study are available from the corresponding author upon reasonable request.

Declaration of competing interest

The authors declare no conflict of interest.

CRediT authorship contribution statement

Dong Uk Lee: Writing – review & editing, Writing – original draft, Visualization, Methodology, Investigation, Formal analysis, Data curation, Conceptualization. **Mukhammad Kayumov:** Writing – original draft, Validation, Methodology, Investigation. **Junghun Park:** Writing – original draft, Resources, Methodology, Investigation, Funding acquisition. **Se Kye Park:** Investigation. **Yeongkwon Kang:** Writing – review & editing, Investigation, Conceptualization. **Yejin Ahn:** Validation, Investigation. **Woojin Kim:** Resources, Methodology. **Seung Hwa Yoo:** Resources. **Jun-Kyu Park:** Methodology. **Bong-Gi Kim:** Resources. **Yong Suk Oh:** Resources. **In-Seok Jeong:** Validation, Supervision, Methodology. **Dong Yun Choi:** Writing – review & editing, Validation, Supervision, Project administration, Methodology, Funding acquisition.

Acknowledgments

D. U. Lee, M. Kayumov and J. Park contributed equally to this work. This work was supported by the Korea Evaluation Institute of Industrial Technology (KEIT) grant funded by the South Korea government (MOTIE) (No. 1415187426, RS-2023-00238181). It was also partly supported by the institutional program funded by the Korea Institute of Industrial Technology (JA230007) and the National Research Foundation of Korea (NRF) grant funded by the South Korea government (MSIT) (No. 2022R1F1A1074255; No. RS-2022-00144435).

Appendix A. Supplementary data

Supplementary data to this article can be found online at <https://doi.org/10.1016/j.bioactmat.2023.12.009>.

References

- [1] World Health Organization (Who), Cardiovascular Diseases (CVDs), 2021. <https://www.who.int/news-room/fact-sheets/detail/cardiovascular-diseases-cvds>.
- [2] P.-S. Yang, D. Kim, J.-H. Sung, E. Jang, H.T. Yu, T.-H. Kim, J.-S. Uhm, J.-Y. Kim, H.-N. Pak, M.-H. Lee, B. Joung, Reduction of mortality by catheter ablation in real-world atrial fibrillation patients with heart failure, *Sci. Rep.* 11 (2021) 4694, <https://doi.org/10.1038/2Fs41598-021-84256-z>.
- [3] V. Chopra, S. Smith, L. Swaminathan, T. Boldenow, S. Kaatz, S.J. Bernstein, S. A. Flanders, Variations in peripherally inserted central catheter use and outcomes in Michigan hospitals, *AMA Intern. Med.* 176 (4) (2016) 548–551, <https://doi.org/10.1001/jamainternmed.2015.8402>.
- [4] J.A. Schults, T. Kleidon, H.L. Petsky, R. Stone, J. Schoutrop, A.J. Ullman, Peripherally inserted central catheter design and material for reducing catheter failure and complications, *Cochrane Database Syst. Rev.* (7) (2019) CD013366, <https://doi.org/10.1002/2F14651858.CD013366>, 2019.
- [5] Y. Lv, X. Huang, Y. Lan, Q. Xia, F. Chen, J. Wu, W. Li, H. Cao, C. Xie, L. Li, H. Han, H. Wang, Q. Xiang, Peripherally inserted central catheters have a protective role and the effect of fluctuation curve feature in the risk of bloodstream infection compared with central venous catheters: a propensity-adjusted analysis, *BMC Infect. Dis.* 22 (2022) 289, <https://doi.org/10.1186/s12879-022-07265-x>.
- [6] N. Fallouh, H.M. McGuiRK, S.A. Flanders, V. Chopra, Peripherally inserted central catheter-associated deep vein thrombosis: a narrative review, *Am. J. Med.* 128 (7) (2015) 722–738, <https://doi.org/10.1016/j.amjmed.2015.01.027>.
- [7] R.M.F. Wagner, R. Maiti, M.J. Carré, C.M. Perrault, P.C. Evans, R. Lewis, Biotribology of vascular devices: a review of tissue/device friction Research, *Biotribology* 25 (2021), 100169, <https://doi.org/10.1016/j.biotri.2021.100169>.
- [8] K. Dellimore, S.E. Franklin, A.R. Helyer, A review of catheter related complications during minimally invasive transcatheter cardiovascular intervention with implications for catheter design, *Cardiovasc. Eng. Technol.* 5 (2014) 217–232, <https://doi.org/10.1007/S13239-014-0183-9>.
- [9] S.I.C. Ricardo, I.L.L. Anjos, N. Monge, C.M.C. Faustino, I.A.C. Ribeiro, A glance at antimicrobial strategies to prevent catheter-associated medical infections, *ACS Infect. Dis.* 6 (12) (2020) 3109–3130, <https://doi.org/10.1021/acsinfectdis.0c00526>.
- [10] M. Al-Qahtani, A. Safan, G. Jassim, S. Abadla, Efficacy of anti-microbial catheters in preventing catheter associated urinary tract infections in hospitalized patients: a review on recent updates, *J. Infect. Public Health* 12 (6) (2019) 760, <https://doi.org/10.1016/j.jiph.2019.09.009>.
- [11] S. Bohara, J. Suthakorn, Surface coating of orthopedic implant to enhance the osseointegration and reduction of bacterial colonization: a review, *Biomater. Res.* 26 (2022) 26, <https://doi.org/10.1186/s40824-022-00269-3>.

- [12] A.H. Benfield, S.T. Henriques, Mode-of-Action of antimicrobial peptides: membrane disruption vs. Intracellular mechanism, *Front. Med. Technol.* 2 (2020), 610997, <https://doi.org/10.3389/fmedt.2020.610997>.
- [13] Y. Okamoto, R. Yano, K. Miyatake, I. Tomohiro, Y. Shigemasa, S. Minami, Effects of chitin and chitosan on blood coagulation, *Carbohydr. Polym.* 53 (3) (2003) 337–342, [https://doi.org/10.1016/S0144-8617\(03\)00076-6](https://doi.org/10.1016/S0144-8617(03)00076-6).
- [14] Y. Bian, K. Kim, T. Ngo, I. Kim, O.N. Bae, K. Lim, J. Chung, Silver nanoparticles promote procoagulant activity of red blood cells: a potential risk of thrombosis in susceptible population, *Part, Fibre Toxicol* 16 (2019) 9, <https://doi.org/10.1186/s12989-019-0292-6>.
- [15] C.D. Hoemann, C. Marchand, G. Rivard, H. El-Gabalawy, P.E. Poubelle, Effect of chitosan and coagulation factors on the wound repair phenotype of bioengineered blood clots, *Int. J. Biol. Macromol.* 104 (part B) (2017) 1916–1924, <https://doi.org/10.1016/j.ijbiomac.2017.04.114>.
- [16] J. Laloy, V. Minet, L. Alpan, F. Mullier, S. Beken, O. Toussaint, S. Lucas, J.-M. Dongné, Impact of silver nanoparticles on haemolysis, platelet function and coagulation, *Nanobiomedicine* 1 (2014) 4, <https://doi.org/10.5772/59346>.
- [17] G.V.F. Seaman, Electrochemical features of platelet interactions, *Thromb. Res.* 8 (1976) 235–246, [https://doi.org/10.1016/0049-3848\(76\)90066-9](https://doi.org/10.1016/0049-3848(76)90066-9).
- [18] B. Furie, B.C. Furie, Mechanisms of thrombus formation, *N. Engl. J. Med.* 359 (9) (2008) 938–949, <https://doi.org/10.1056/nejmra0801082>.
- [19] D.U. Lee, D.W. Kim, S.Y. Lee, D.Y. Choi, S.Y. Choi, K. Moon, M.Y. Shon, M.J. Moon, Amino acid-mediated negatively charged surface improve antifouling and tribological characteristics for medical applications, *Colloids Surf. B Biointerfaces* 211 (2022), 112314, <https://doi.org/10.1016/j.colsurfb.2021.112314>.
- [20] S.K. Park, J.H. Shin, J.H. Jung, D.Y. Lee, D.Y. Choi, S.H. Yoo, Polysaccharide-derivative coated intravascular catheters with superior multifunctional performance via simple and biocompatible method, *Chem. Eng. J.* 433 (part 1) (2022), 134565, <https://doi.org/10.1016/j.cej.2022.134565>.
- [21] R. Biran, D. Pond, Heparin coatings for improving blood compatibility of medical devices, *Adv. Drug Deliv. Rev.* 112 (2017) 12–23, <https://doi.org/10.1016/j.addr.2016.12.002>.
- [22] R. Jayakumar, M. Prabaharan, S.V. Nair, S. Tokura, H. Tamura, N. Selvamurugan, Novel carboxymethyl derivatives of chitin and chitosan materials and their biomedical applications, *Prog. Mater. Sci.* 55 (7) (2010) 675–709, <https://doi.org/10.1016/j.pmatsci.2010.03.001>.
- [23] W. Zhang, D. Zhong, Q. Liu, Y. Zhang, N. Li, Q. Wang, Z. Liu, W. Xue, Effect of chitosan and carboxymethyl chitosan on fibrinogen structure and blood coagulation, *J. Biomater. Sci. Polym.* 24 (13) (2013) 1549–1563, <https://doi.org/10.1080/09205063.2013.777229>.
- [24] T. Xiang, T. Lu, Y. Xie, W. Zhao, S. Sun, C. Zhao, Zwitterionic polymer functionalization of polysulfone membrane with improved antifouling property and blood compatibility by combination of ATRP and click chemistry, *Acta Biomater.* 40 (2016) 162–171, <https://doi.org/10.1016/j.actbio.2016.03.044>.
- [25] L. Yang, H. Wu, Y. Liu, Q. Xia, Y. Yang, N. Chen, M. Yang, R. Luo, G. Liu, Y. Wang, A robust mussel-inspired zwitterionic coating on biodegradable poly (L-lactide) stent with enhanced anticoagulant, anti-inflammatory, and anti-hyperplasia properties, *Chem. Eng. J.* 427 (2022), 130910, <https://doi.org/10.1016/j.cej.2021.130910>.
- [26] J. Wu, S. Chen, Investigation of the hydration of nonfouling material poly(ethylene glycol) by low-field nuclear magnetic resonance, *Langmuir* 28 (4) (2012) 2137–2144, <https://doi.org/10.1021/la203827h>.
- [27] H. Chen, J. Yang, S. Xiao, R. Hu, S.M. Bhaway, B.D. Vogt, M. Zhang, Q. Chen, J. Ma, Y. Chang, L. Li, J. Zheng, Salt-responsive polyzwitterionic materials for surface regeneration between switchable fouling and antifouling properties, *Acta Biomater.* 40 (2016) 62–69, <https://doi.org/10.1016/j.actbio.2016.03.009>.
- [28] R.I. Mehta, R.I. Mehta, Hydrophilic polymer embolism: implications for manufacturing, regulation, and postmarket surveillance of coated intravascular medical devices, *J. Patient Saf.* 17 (8) (2021) e1069–e1079, <https://doi.org/10.1097/pts.0000000000000473>.
- [29] C. Lin, H. Wan, H.J. Kaper, P.K. Sharma, A hyaluronic acid based lubricious coating for cardiovascular catheters, *Tribol. Int.* 151 (2020), 106495, <https://doi.org/10.1016/j.triboint.2020.106495>.
- [30] L. Capron, P. Bruneval, Influence of applied stress on mitotic response of arteries to injury with a balloon catheter: quantitative study in rat thoracic aorta, *Cardiovasc. Res.* 23 (11) (1989) 941–948, <https://doi.org/10.1093/cvr/23.11.941>.
- [31] D.U. Lee, S. Kim, D.Y. Choi, W. Jung, M.J. Moon, Basic amino acid-mediated cationic amphiphilic surfaces for antimicrobial pH monitoring sensor with wound healing effects, *Biomater. Res.* 27 (2023) 14, <https://doi.org/10.1186/s40824-023-00355-0>.
- [32] M. Johansson, A.C. Eriksson, C.J. Östgren, P.A. Whiss, Platelet adhesion in type 2 diabetes: impact of plasma albumin and mean platelet volume, *Thromb. J.* 19 (2021) 40, <https://doi.org/10.1186/s12959-021-00291-w>.
- [33] X. Jia, C. Hua, F. Yang, X. Li, P. Zhao, F. Zhou, Y. Lu, H. Liang, M. Xing, G. Lyu, Hydrophobic aerogel-modified hemostatic gauze with thermal management performance, *Bioact. Mater.* 26 (2023) 142–158, <https://doi.org/10.1016/j.bioactmat.2023.02.017>.
- [34] T.A. Halgren, Merck molecular force field. I. Basis, form, scope, parameterization, and performance of MMFF94, *J. Comput. Chem.* 17 (5–6) (1996) 490–519, [https://doi.org/10.1002/\(SICI\)1096-987X\(199604\)17:5<63AC490::AID-JCC1%3E3.0.CO;2-P](https://doi.org/10.1002/(SICI)1096-987X(199604)17:5<63AC490::AID-JCC1%3E3.0.CO;2-P).
- [35] D.A. Murguía-Flores, J. Bonilla-Ríos, M.R. Canales-Fiscal, A. Sánchez-Fernández, Protein adsorption through Chitosan–Alginate membranes for potential applications, *Chem. Cent. J.* 10 (2016) 26, <https://doi.org/10.1186/s13065-016-0167-y>.
- [36] S. Singh, T. Taketsugu, R.K. Singh, Hydration, prediction of the pKa, and infrared spectroscopic study of sulfonated polybenzophenone (SPK) block-copolymer hydrocarbon membranes and comparisons with nafion, *ACS Omega* 6 (48) (2021) 32739–32748, <https://doi.org/10.1021/acsomega.1c04484>.
- [37] S.F.B. Ibrahim, N.A.N.M. Azam, K.A.M. Amin, Sodium alginate film: the effect of crosslinker on physical and mechanical properties, *IOP Conf. Ser. Mater. Sci. Eng.* 509 (2019), 012063, <https://doi.org/10.1088/1757-899X/509/1/012063>.
- [38] F.V. Ferreira, L.P. Souza, T.M.M. Martins, J.H. Lopes, B.D. Mattos, M. Mariano, I. F. Pinheiro, T.M. Valverde, S. Livi, J.A. Camilli, A.M. Goes, R.F. Gouveia, L.M. F. Lona, O.J. Rojas, Nanocellulose/bioactive glass cryogels as scaffolds for bone regeneration, *Nanoscale* 11 (2019), <https://doi.org/10.1039/C9NR05383B>, 19842–19489.
- [39] M. Yao, H. Sun, Z. Guo, X. Sun, Q. Yu, X. Wu, C. Yu, H. Zhang, F. Yao, J. Li, A starch-based zwitterionic hydrogel coating for blood-contacting devices with durability and bio-functionality, *Chem. Eng. J.* 421 (part 1) (2021), 129702, <https://doi.org/10.1016/j.cej.2021.129702>.
- [40] T. Xiang, L.-S. Zhang, R. Wang, Y. Xia, B.-H. Su, C.-S. Zhao, Blood compatibility comparison for polysulfone membranes modified by grafting block and random zwitterionic copolymers via surface-initiated ATRP, *J. Colloid Interface Sci.* 432 (2014) 47–56, <https://doi.org/10.1016/j.jcis.2014.06.044>.
- [41] V. Shutthanandan, M. Nandasiri, J. Zheng, M.H. Engelhard, W. Xu, S. Thevuthasan, V. Murugesan, Applications of XPS in the characterization of Battery materials, *J. Electron. Spectrosc. Relat. Phenom.* 231 (2019) 2–10, <https://doi.org/10.1016/j.jelspec.2018.05.005>.
- [42] D.Y. Choi, M.H. Kim, Y.S. Oh, S.H. Jung, J.H. Jung, H.J. Sung, H.W. Lee, H.M. Lee, Highly stretchable, hysteresis-free ionic liquid-based strain sensor for precise human motion monitoring, *ACS Appl. Mater. Interfaces* 9 (2) (2017) 1770–1780, <https://doi.org/10.1021/acsaami.6b12415>.
- [43] T. Chen, R. Wang, L.Q. Xu, K.G. Neoh, E.-T. Kang, Carboxymethyl chitosan-functionalized magnetic nanoparticles for disruption of biofilms of *Staphylococcus aureus* and *Escherichia coli*, *Ind. Eng. Chem. Res.* 51 (40) (2012) 13164–13172, <https://doi.org/10.1021/ie301522w>.
- [44] C. Yang, M. Long, C. Ding, et al., Antifouling graphene oxide membranes for oil-water separation via hydrophobic chain engineering, *Nat. Commun.* 13 (2022) 7334, <https://doi.org/10.1038/s41467-022-35105-8>.
- [45] R. Wang, X. Song, T. Xiang, Q. Liu, B. Su, W. Zhao, C. Zhao, Mussel-inspired chitosan-polyurethane coatings for improving the antifouling and antibacterial properties of polyethersulfone membranes, *Carbohydr. Polym.* 168 (2017) 310–319, <https://doi.org/10.1016/j.carbpol.2017.03.092>.
- [46] Q. Shao, L. Mi, X. Han, T. Bai, S. Liu, Y. Li, S. Jiang, Differences in cationic and anionic charge densities dictate zwitterionic associations and stimuli responses, *J. Phys. Chem. B* 118 (24) (2014) 6956–6962, <https://doi.org/10.1021/jp503473u>.
- [47] J.T. Willerson, P. Golino, J. Eidt, W.B. Cambell, L.M. Buja, Specific platelet mediators and unstable coronary artery lesions. Experimental evidence and potential clinical implications, *Circulation* 80 (1989) 198–205, <https://doi.org/10.1161/01.CIR.80.1.198>.
- [48] X.R. Xu, N. Carrim, M.A.D. Neves, T. McKeown, T.W. Stratton, R.M.P. Coelho, X. Lei, P. Chen, J. Xu, X. Dai, B.X. Li, H. Ni, Platelets and platelet adhesion molecules: novel mechanisms of thrombosis and anti-thrombotic therapies, *Thromb. J.* 14 (2016) 29, <https://doi.org/10.1186/s12959-016-0100-6>.
- [49] A.P. Wheeler, D. Gailani, The intrinsic pathway of coagulation as a target for antithrombotic therapy, *Hematol. Oncol. Clin. N. Am.* 30 (5) (2016) 1099–1114, <https://doi.org/10.1016/j.hoc.2016.05.007>.
- [50] S.E. Reitsma, J. Pang, V. Raghunathan, J.J. Shatzel, C.U. Lorentz, E.I. Tucker, A. Gruber, D. Gailani, O.J.T. McCarty, C. Puy, Role of platelets in regulating activated coagulation factor XI activity, *Am. J. Physiol. Cell Physiol.* 320 (3) (2021) C363–C374, <https://doi.org/10.1152/ajpcell.00056.2020>.
- [51] N. Mackman, R.E. Tilley, N.S. Key, Role of the extrinsic pathway of blood coagulation in hemostasis and thrombosis, *Arterioscler. Thromb. Vasc. Biol.* 27 (2007) 1687–1693, <https://doi.org/10.1161/ATVBAHA.107.141911>.
- [52] J. Rosing, J.L.V. Rijn, E.M. Bevers, G.V. Dieijen, P. Comfurius, R.F. Zwaal, The role of activated human platelets in prothrombin and factor X activation, *Blood* 65 (2) (1985) 319–332, <https://doi.org/10.1182/blood.V65.2.319.319>.
- [53] C.F. Wertz, M.M. Santore, Adsorption and relaxation kinetics of albumin and fibrinogen on hydrophobic surfaces: single-species and competitive behavior, *Langmuir* 15 (26) (1999) 8884–8894, <https://doi.org/10.1021/la990089q>.
- [54] C. Lin, H.J. Kaper, W. Li, R. Splinter, P.K. Sharma, Role of endothelial glycocalyx in sliding friction at the catheter-blood vessel interface, *Sci. Rep.* 10 (1) (2020), 11855, <https://doi.org/10.1038/s41598-020-68870-x>.
- [55] K.M. Naegeli, M.H. Kural, Y. Li, J. Wang, E.A. Hugentobler, L.E. Niklason, Bioengineering human tissues and the future of vascular replacement, *Circ. Res.* 131 (2022) 109–126, <https://doi.org/10.1161/CIRCRESAHA.121.319984>.